CELL BIOLOGY

Late endosomes promote microglia migration via cytosolic translocation of immature protease cathD

Yi-Jun Liu[1]*, Ting Zhang[1], Daxiao Cheng[1], Junhua Yang[1], Sicong Chen[2], Xingyue Wang[1], Xia Li[1], Duo Duan[1], Huifang Lou[1], Liya Zhu[1], Jianhong Luo[1], Margaret S. Ho[3]*, Xiao-Dong Wang[1,4]*, Shumin Duan[1,5]*

Organelle transport requires dynamic cytoskeleton remodeling, but whether cytoskeletal dynamics are, in turn, regulated by organelles remains elusive. Here, we demonstrate that late endosomes, a type of prelysosomal organelles, facilitate actin-cytoskeleton remodeling via cytosolic translocation of immature protease cathepsin D (cathD) during microglia migration. After cytosolic translocation, late endosome–derived cathD juxtaposes actin filaments at the leading edge of lamellipodia. Suppressing cathD expression or blocking its cytosolic translocation impairs the maintenance but not the initiation of lamellipodial extension. Moreover, immature cathD balances the activity of the actin-severing protein cofilin to maintain globular-actin (G-actin) monomer pool for local actin recycling. Our study identifies cathD as a key lysosomal molecule that unconventionally contributes to actin cytoskeleton remodeling via cytosolic translocation during adenosine triphosphate–evoked microglia migration.

INTRODUCTION

Endosome/lysosomes are cellular recycling centers filled with potent acidic hydrolases. Upon severe damage or membrane rupture, endosome/lysosomes release hydrolases into the cytosol to trigger cell death, making them the long-considered "suicide bags" in cells (1). However, most intracellularly released hydrolases lose their catalytic activities after arriving at the neutral pH cytosol, making them insufficient to kill cells upon minor lysosomal leakage (2). Furthermore, recent studies show that partial or minor rupture of endosomal/lysosomal membrane can be repaired by endogenous machineries (3, 4), suggesting that restricted endosomal/lysosomal leakage might be common cellular events with physiological importance. In addition, it has been reported that lysosomal hydrolases in cytosol enhance cell motility (5–7), whereas impaired lysosomal integrity facilitates exosome secretion and cancer cell invasion (8). These findings implicate potentially broader roles of endosome/lysosomes beyond proteolytic activities.

In fast-moving cells such as neutrophils, monocytes, and macrophages, robust rearrangements of actin cytoskeleton combined with weak adhesions permit rapid amoeboid movement (9). A similar crawling pattern can also be found in tumor cell migration (10, 11). Intriguingly, these motile cells are enriched with endosomal/lysosomal vesicles containing abundant acidic hydrolases in general (12). In the central nervous system, the amoeboid-like cell motility of microglia can be driven by purinergic signals especially adenosine triphosphate (ATP) released from damaged tissue (13–15). In response to injury or infection, lysosome-enriched microglia rapidly generate actin-based lamellipodia moving toward the stimuli to clean up pathological

contexts (16, 17). Disruption of endosome/lysosome abolishes ATP-evoked microglia migration (18). However, the regulatory role of endosome/lysosomes in cell migration is still poorly understood.

Here, we report that late endosomes regulate cytoskeleton reorganization via cytosolic translocation of immature lysosomal hydrolase cathepsin D (cathD) during microglia migration. By intracellular release of immature cathD, late endosomes coordinate leading edge dynamics and promote amoeboid-like migration via replenishing local G-actin pool. Furthermore, down-regulation of cathD or blocking late endosome permeabilization impairs the balance of cofilin activity and actin cytoskeleton remodeling in lamellipodia extension, indicating that immature cathD also serves as a regulator of the actin cytoskeleton when translocated to the cytosol. Together, these results demonstrate a previously unidentified role of late endosomes in regulating actin-driven lamellipodial extension in ATP signaling–evoked microglia migration.

RESULTS

Late endosomes release immature cathD intracellularly during migration

To identify key endosomal/lysosomal molecules regulating rapid microglia migration, primary microglia were treated with non-hydrolyzable adenosine 5′-O-(3-thiotriphosphate) (ATP-γ-S) to evoke actin-based protrusions and examined for the spatial distribution of endosomal/lysosomal components. Among all candidates, the protease cathD exhibited a mixed punctate/diffused pattern within cell bodies and colocalized with the phalloidin-labeled F-actin lamellipodia at microglial leading edge (Fig. 1A and movie S1). Intriguingly, labeling the entire cell periphery with the CM-DiI dye together with cathD revealed a strong overlap only at the leading edge (fig. S1A). Considering that lamellipodia-distributed cathD markedly increased after ATP-γ-S stimulation (fig. S1B), these results suggest that cathD translocates to the lamellipodia at the leading edge during ATP signaling–evoked microglia migration.

Since lamellipodia are thin sheet-like protrusions devoid of major organelles, we next determined the precise subcellular location of cathD at lamellipodia. During lamellipodia formation and extension,

[1]Department of Neurobiology, NHC and CAMS Key Laboratory of Medical Neurobiology, School of Brain Science and Brian Medicine, and the MOE Frontier Science Center for Brain Research and Brain-Machine Integration, Zhejiang University School of Medicine, Hangzhou 310058, China. [2]Clinical Research Center, The Second Affiliated Hospital, Zhejiang University School of Medicine, Hangzhou 310009, China. [3]School of Life Science and Technology, ShanghaiTech University, Shanghai 201210, China. [4]Department of Psychiatry, Sir Run Run Shaw Hospital, Zhejiang University School of Medicine, Hangzhou 310016, China. [5]Mental Health Center, Zhejiang University School of Medicine, Hangzhou, China.
*Corresponding author. Email: duanshumin@zju.edu.cn (S.D.); xiaodongwang@zju.edu.cn (X.-D.W.); margareth@shanghaitech.edu.cn (M.S.H.); yjliu@zju.edu.cn (Y.-J.L.)
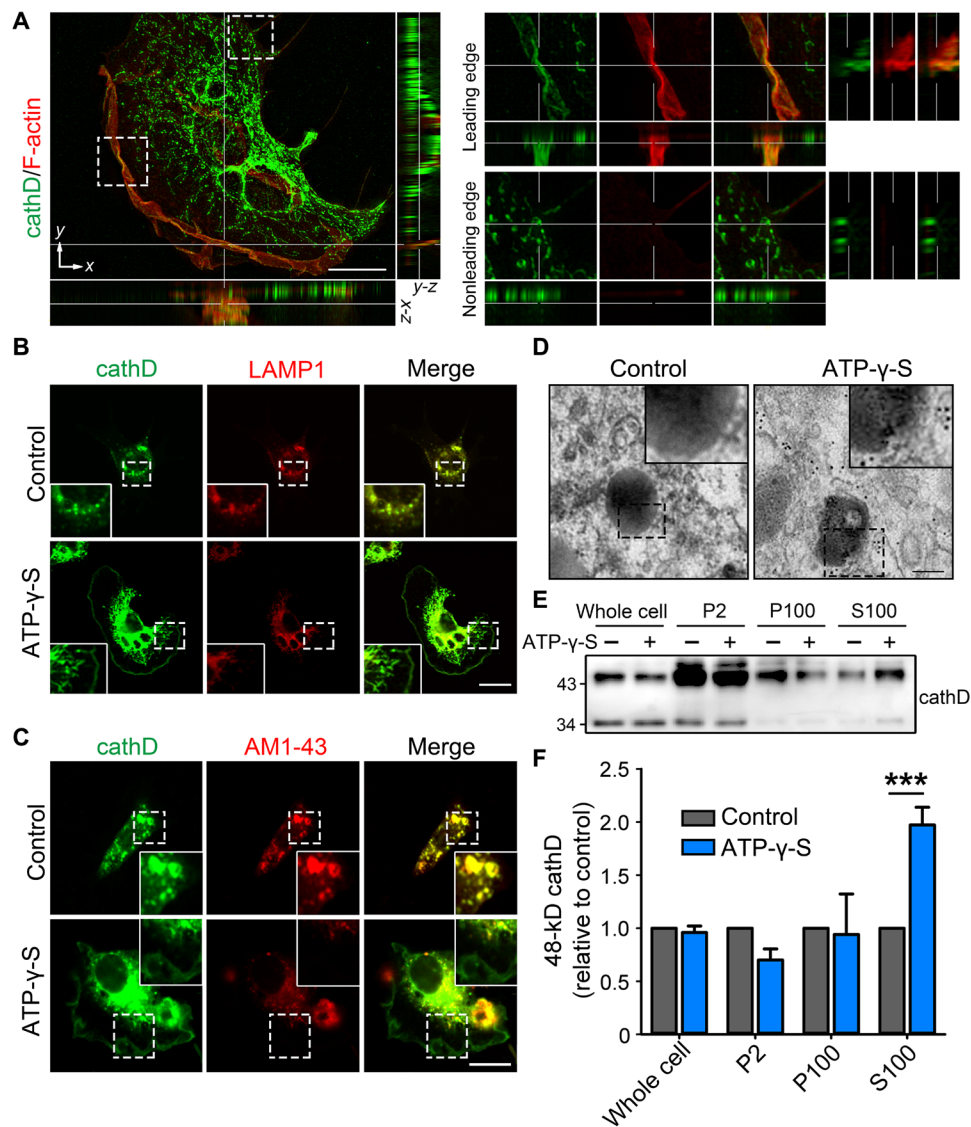
Fig. 1. Late endosomes release immature cathD during fast migration. (**A**) Translocation of cathD to the leading edge was examined by structured illumination microscopy, showing that cathD colocalizes with the F-actin network only at the leading edge of migrating microglia (colocalization coefficient, $r = 0.91 \pm 0.028$, $n = 9$). (**B** and **C**) Control or ATP-γ-S–stimulated migrating microglia were costained for cathD and indicated vesicular markers. (**D**) Representative electron micrographs showing that nanogold particles (5 nm)–labeled cathD exists in the cytosol around late endosomal/lysosomal vesicles after ATP-γ-S treatment. (**E**) Whole-cell, P2 (vacuolar), P100 (membrane), and S100 (cytosolic) fractions from control and ATP-γ-S–treated microglia were analyzed by immunoblotting using indicated antibodies. A representative blot is shown. (**F**) Quantifications of data in (E), revealing an increase of the immature 48-kDa cathD in the cytosolic fraction in ATP-γ-S–treated cells. In all micrographs, the boxed areas are magnified in the insets. In all fluorescence micrographs, coincidence of green and red appears yellow. Scale bars, 10 μm (A to C), 200 nm (D), and z-step is 10 μm (A). Data are shown as means ± SEM, ***$P < 0.001$ by one-way analysis of variance (ANOVA) with Newman-Keuls multiple comparison test.

LysoTracker-labeled acidic vesicles trafficked randomly within the cell body and rarely appeared at the leading edge (movie S2). Costaining results confirmed that cathD at the leading edge did not colocalize with EEA1 (early endosome antigen 1)–labeled early endosomes, lysosome-associated membrane protein type 1 (LAMP1)–labeled late endosome/lysosomes, or the AM1-43-positive endocytic and exocytic vesicles upon ATP-γ-S stimulation (Fig. 1, B and C, and fig. S1C). Furthermore, cathD remained at the lamellipodia of leading edge after ATP-γ-S stimulation in microglia deficient of Rab27a (Ras-related protein Rab-27a), a small guanosine triphosphatase required for granule docking in exocytosis, indicating that lamellipodia cathD does not undergo exocytosis (fig. S1, D and E) (19–21). Together,

these results suggest that lamellipodia-distributed cathD is intracellularly released and escapes from endosome/lysosomes.

To verify our assumption, pre-embedding immunoelectron microscopy was performed to visualize cytosolic proteins (22). In our observation, gold particle–labeled cathD appeared around endosome/lysosome-related organelles, indicative of cathD cytosolic translocation during ATP-γ-S–triggered migration (Fig. 1D). To confirm these results, cytosolic components isolated by differential centrifugation were analyzed for cathD presence in each fraction. Notably, protein levels of the immature 48-kDa cathD (the late-endosomal intermediate form) were elevated in the cytosolic fraction (S100) upon ATP-γ-S stimulation (Fig. 1, E and F). Among all cathepsins

detected, cathD protein levels were uniquely increased in the cytosol, especially its 48-kDa intermediate form (fig. S1, F to H), which is stored in late endosomes before complete maturation (*23*). These results suggest that the immature 48-kDa cathD is transferred from late endosomes to cytosol and presents at the lamellipodia leading edge during ATP-evoked fast migration.

CathD controls actin-mediated lamellipodia extension

The unique lamellipodia localization of cathD drove us to examine its function at the leading edge. We applied cathD inhibitors before evoking microglia migration followed by F-actin staining. Notably, ATP-γ-S–evoked lamellipodia extension was suppressed by pepstatin A and other cathD inhibitors in a dose-dependent manner (Fig. 2, A and B). Similar effects were also detected after cathD knockdown by RNA interference or gene depletion (Fig. 2, C to F). These results suggest a pivotal role of cathD in regulating lamellipodia dynamics. Therefore, cathD is probably a key player in the remodeling of actin cytoskeleton.

During cell migration, coordinated actin dynamics generate protrusive force to constantly push the leading edge forward. On the basis of a treadmilling cycle, G-actin monomers are polymerized at the barbed end to elongate actin filaments, while depolymerization simultaneously occurs at the pointed end to maintain the local G-actin pool (*24*). To better understand the role of cathD in regulating actin dynamics, the overall population of F-actin and G-actin in migrating cells was examined. An increase in F-actin levels was noticed in wild-type microglia, whereas no obvious change in F-actin levels was observed in cathD-deficient microglia upon ATP-γ-S stimulation, suggesting that cathD depletion disrupts actin assembly during microglia migration (Fig. 2, G and H). Together, cathD regulates actin-based lamellipodia extension during ATP-evoked migration.

Cytosolic translocation of cathD is required for leading edge dynamics

To investigate the mechanism of ATP-γ-S–induced cathD cytosolic translocation, the endosome/lysosome integrity was analyzed using a real-time imaging method as previously described (*25*). Labeled with a fluorescent pH-indicator acridine orange (AO), acidic vesicles become sensitive to light-induced photo-oxidation, which results in cytosolic leakage and subsequent shifts of AO fluorescence upon blue light exposure. By analyzing the fluorescence shift of AO, the endosomal/lysosomal membrane permeability can be determined during migration. Upon photo-oxidation, ATP-γ-S stimulation accelerated the decay of red fluorescence and the raise of green fluorescence in primary microglia, respectively (Fig. 3, A and B), suggesting an increase in endosomal/lysosomal membrane permeability during ATP-evoked migration.

To identify the potential role of purinergic receptors and related downstream signaling pathways, microglia were incubated with purinergic receptor antagonists or downstream signal inhibitors before AO labeling and ATP-γ-S stimulation. Notably, endosomal/lysosomal membrane permeability was reverted to the control level in the presence of MRS2395 (2,2-Dimethyl-propionic acid 3-(2-chloro-6-methylaminopurin-9-yl)-2-(2,2-dimethyl-propionyloxymethyl)-propyl ester) (a $P2Y_{12}R$ antagonist) or wortmannin [a phosphatidylinositol 3-kinase (PI3K) inhibitor; Fig. 3B], suggesting that ATP-$P2Y_{12}R$ (receptor)–PI3K signaling pathway controls endosomal/lysosomal membrane permeability and increases the probability for cathD cytosolic translocation.

Heat-shock protein 70 (Hsp70), a stress-inducible chaperone, decreases endosomal/lysosomal permeability by stabilizing their membranes (*25*, *26*). To further demonstrate that cathD translocates to the cytosol from endosome/lysosomes, microglia were incubated with recombinant human Hsp70 (rHsp70) to block cytosolic translocation, and the subsequent effect on lamellipodia extension upon ATP stimulation was analyzed. Immunostaining results showed that cathD was present as puncta-like structures within cell bodies and no longer colocalized with F-actin at the cell periphery in the presence of rHsp70 (Fig. 3C). Furthermore, ATP-γ-S–evoked lamellipodia extension was markedly reduced by rHsp70 pretreatment as indicated by the absence of F-actin staining at the leading edge (Fig. 3C and fig. S2A). These results suggest that cathD cytosolic translocation and consequent lamellipodia extension are regulated by Hsp70-controlled endosomal/lysosomal membrane permeability.

We further investigated whether weakened integrity of endosome/lysosomes promotes cell motility. To address this issue, BV2 microglial cell line, which expresses multiple purinergic receptors but displays much slower dynamics than primary microglia upon ATP-γ-S stimulation, was treated with a potent Hsp70 inhibitor (HSP inhibitor I) to sensitize endosomal/lysosomal membrane and enhance potential cytosolic translocation, followed by ATP-γ-S stimulation and F-actin staining. Our results showed that Hsp70 inhibition increased lamellipodial growth and enhanced cell motility upon ATP-γ-S stimulation, suggesting that weakened integrity of endosome/lysosomes facilitates lamellipodia extension and cell motility (fig. S2, B and C). Conversely, lamellipodia extension of primary microglia was blocked by Hsp70-mediated stabilization of endosomal/lysosomal membranes upon ATP-γ-S stimulation, implicating that Hsp70-associated endosomal/lysosomal integrity is essential for regulating lamellipodia dynamics (fig. S2D). Therefore, Hsp70-controlled endosomal/lysosomal integrity plays an important role during cathD cytosolic translocation and lamellipodia extension in microglia.

CathD is required for the maintenance of lamellipodial extension

In light of its role in controlling lamellipodia extension, we then asked whether cathD would affect the initial formation of lamellipodia or subsequent steps during cell migration. To distinguish between these two possibilities, lamellipodia dynamics of the wild-type and cathD-deficient microglia were monitored in real time. As expected, wild-type microglia constantly extend their lamellipodia upon ATP-γ-S stimulation. In the absence of cathD, however, the protrusion persistence was much shorter than wild-type controls (Fig. 3, D and E, and movies S3 and S4). Tracking the membrane dynamics of ATP-γ-S–stimulated microglia showed a remarkable decrease in protrusion magnitude over time in the absence of cathD (Fig. 3D). Similar results were obtained in microglia pretreated with rHsp70 (Fig. 3E and movie S5). Kymograph analysis suggested that the protruded distance and duration of lamellipodia extension were decreased in cathD-deficient microglia after ATP-γ-S stimulation, whereas the protrusion rate, retracted distance, and duration were increased (Fig. 3, F to H, and fig. S2, E and F). No notable difference in the rate of lamellipodia retraction was detected in either control or cathD-deficient microglia (fig. S2G). Microglia incubated with rHsp70 showed similar changes in these protrusion and retraction parameters (Fig. 3, F to H, and fig. S2, E and F). In toto, these results suggest that cathD is required to maintain lamellipodia extension but does not significantly affect the initial formation of these protrusions.
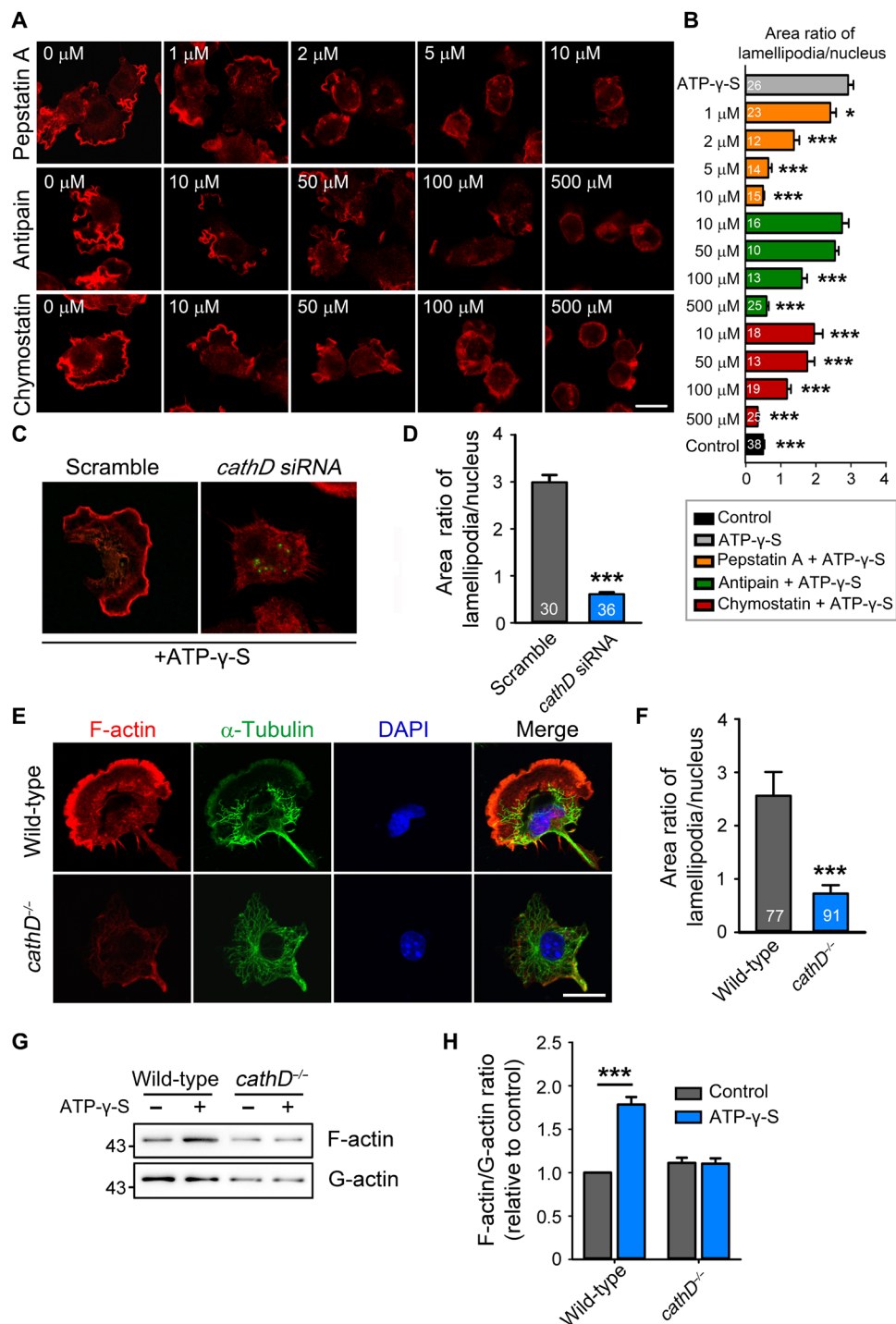
Fig. 2. CathD controls actin-mediated lamellipodia extension. (**A**) Representative images of F-actin staining, showing dosage-dependent inhibition of lamellipodia extension by preincubation of indicated cathD inhibitors (for 4 hours) during ATP-γ-S–evoked microglia migration. Scale bar, 10 μm. (**B**) Quantification of the lamellipodia extension by calculating the ratio of F-actin–positive area (lamellipodia) over the 4′,6-diamidino-2-phenylindole (DAPI)–positive area (nucleus) in each cell in (A). (**C** and **D**) Representative images (C) and quantifications (D) of ATP-γ-S–induced lamellipodia in control and *cathD* siRNA-treated microglia. Scale bar, 10 μm. (**E** and **F**) Represent-ative images (E) and quantifications (F) of ATP-γ-S–induced lamellipodia in wild-type and *cathD*-deficient (*cathD$^{-/-}$*) microglia. Scale bar, 10 μm. (**G** and **H**) ATP-γ-S–induced global changes in F-actin and G-actin levels were analyzed by Western blotting in WT and *cathD* KO microglia. Note that both F-actin and G-actin levels were not affected by ATP-γ-S treatment in *cathD* KO microglia. Data are shown as means ± SEM. *$P < 0.05$ and ***$P < 0.001$ by unpaired student *t* test or one-way ANOVA with Newman-Keuls multiple comparison test among three groups or above.
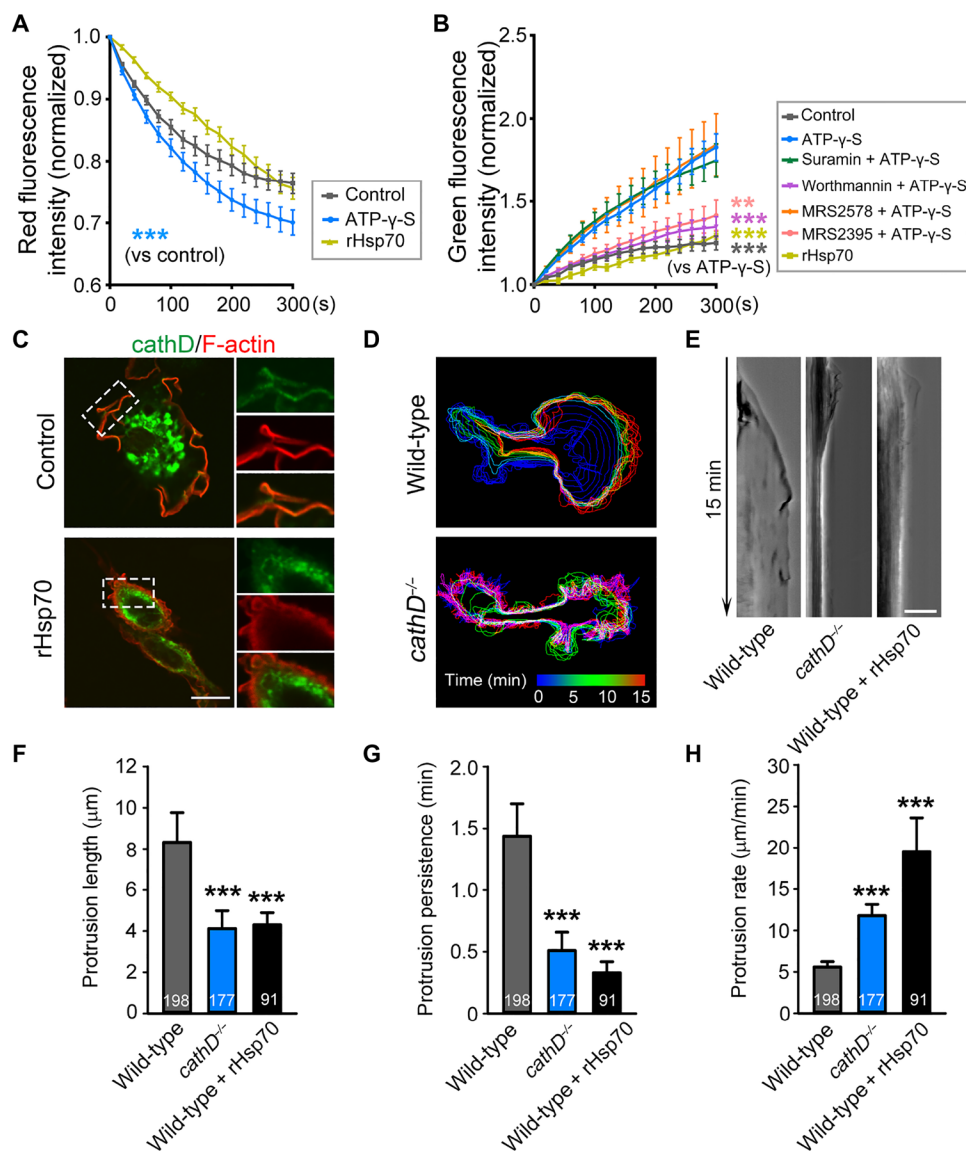
Fig. 3. Cytosolic translocation of cathD is required for lamellipodia maintenance. (**A** and **B**) Microglia were preincubated with inhibitors suramin (5 µM), MRS2395 (20 µM), MRS2578 (2 µM), wortmannin (500 nM), and the vehicle control for 30 min or recombinant human Hsp70 (rHsp70; 300 nM) for 12 hours, followed with AO (2 µg/ml) staining for 15 min. Lysosomal integrity was monitored upon 488-nm laser exposure in control and ATP-γ-S–stimulated microglia. Accelerated decline of lysosomal red fluorescence in (A) and accelerated rise of cytosolic/nuclear green fluorescence in (B), reflecting that ATP-γ-S stimulation enhances endosomal/lysosomal membrane permeability. The retarded rise of cytosolic/nuclear green fluorescence, showing that the loss of lysosomal integrity was blocked by MRS2935 or wortmannin (B). At least 120 cells were examined for each experiment. Each group was compared with ATP-γ-S treatment alone. (**C**) Preincubated with rHsp70 (300 nM) or vehicle for 12 hours, microglia were treated with 10 µM ATP-γ-S for 5 min to induce lamellipodia. Immunofluorescence images showing that cathD exhibits puncta-like pattern and no longer overlapped with F-actin in shrinking lamellipodia. Scale bar, 10 µm. (**D**) Dynamic changes of cell shapes were outlined with different colors in both control and cathD KO microglia upon ATP-γ-S stimulation: blue traces for a time window of 0 to 5 min, green for 5 to 10 min, and red for 10 to 15 min. (**E**) Kymograph analysis of live-imaged lamellipodia protrusions, showing that microglia failed to maintain the ATP-γ-S–induced lamellipodia in the absence of cathD or in the presence of rHsp70. (**F** to **H**) Quantifications of protrusion length (F), persistence (G), and rate (H) in ATP-γ-S–induced lamellipodia. Data are shown as means ± SEM, from 286 to 606 events in a minimum of 90 cells per group. **$P < 0.01$ and ***$P < 0.001$ by Student's t test or one-way ANOVA with Newman-Keuls test among three groups or above.

Cytosolic cathD nonproteolytically balances cofilin activity

To explore the role of cathD in actin dynamics, possible binding partners of cathD were screened by immunoprecipitation coupled with liquid chromatography–tandem mass spectrometry (LC-MS/MS). Validated by coimmunoprecipitation (Co-IP) analysis and immunostaining, cathD interacted with the actin-severing factor cofilin (Fig. 4A), whose activity is essential for generating free G-actin. As the terminal mediator of actin cytoskeletal rearrangement, cofilin is activated by dephosphorylation on its Ser[3] residue (27). In our observation, both total cofilin and inactive phosphorylated cofilin (p-cofilin) colocalized with cathD at the microglia leading edge upon ATP-γ-S stimulation (Fig. 4, B and C). Intriguingly, p-cofilin levels were specifically elevated in protein extracts collected from cathD-deficient microglia, suggesting that cathD is required for balancing cofilin phosphorylation and dephosphorylation during ATP-γ-S–evoked migration (Fig. 4, D and E).
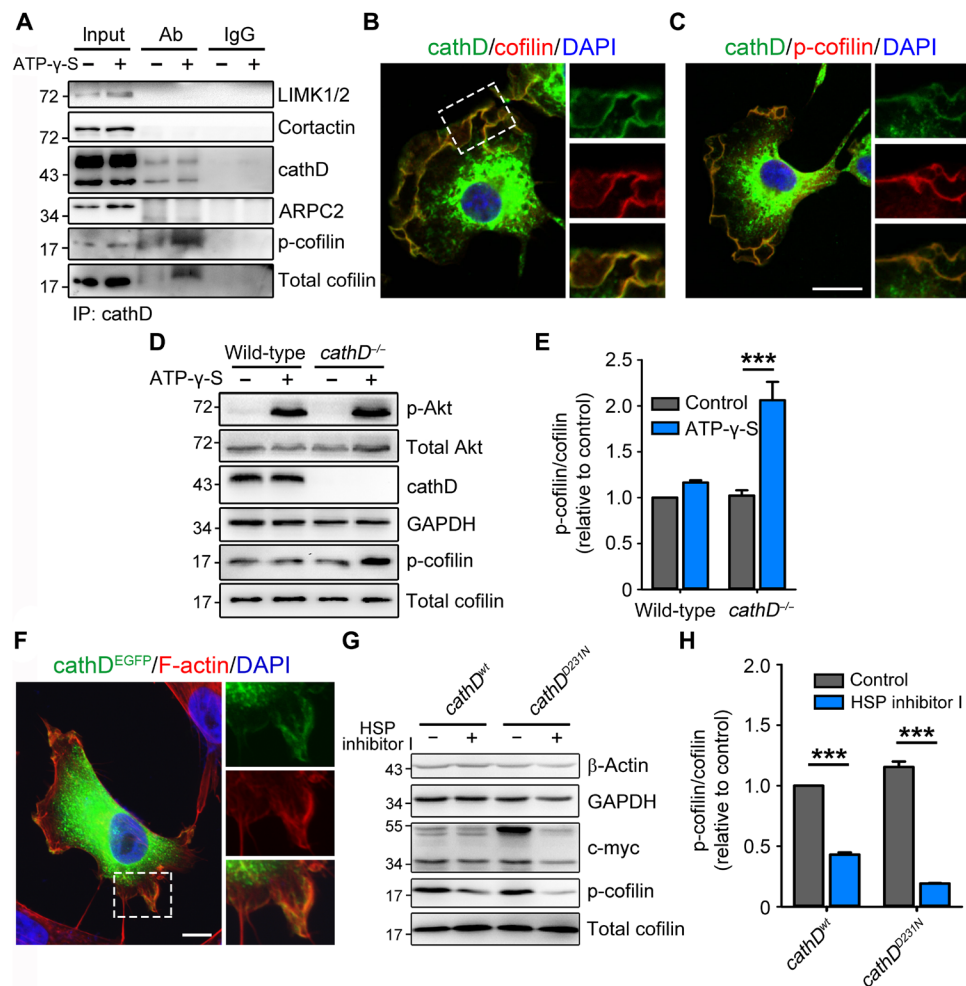
Fig. 4. Cytosolic cathD nonproteolytically balances cofilin activity. (A) Total protein from control or ATP-γ-S–treated microglia was subjected to immunoprecipitation (IP) as described in Materials and Methods. Representative images showing that cathD interacted with cofilin, but not LIMK1, cortactin, or ARPC2 in ATP-γ-S–treated microglia. Ab, antibody; IgG, immunoglobulin G; LIMK1, LIM domain; ARPC2, actin related protein 2/3 complex subunit 2. **(B and C)** Immunofluorescence images showing that peripheral cathD colocalizes with total cofilin (B; colocalization coefficient, $r = 0.76 \pm 0.118$, $n = 7$) and phosphorylated cofilin (p-cofilin) (C; colocalization coefficient, $r = 0.818 \pm 0.099$, $n = 7$) at the lamellipodia in ATP-γ-S–treated microglia. Scale bar, 10 μm. **(D and E)** Representative immunoblot images (D) and quantifications (E) of the indicated proteins levels in cell lysates from wild-type or cathD-deficient microglia, showing an increase in p-cofilin levels in cathD-deficient microglia upon ATP-γ-S stimulation. **(F)** CathD-EGFP–transfected HeLa cells were incubated with Hsp70 inhibitor for 4 hours to induce endosomal/lysosomal membrane permeability, followed with F-actin and DAPI staining. Representative images showing a periphery distribution of cathD in the F-actin–labeled lamellipodia. Scale bar, 10 μm. **(G)** Human embryonic kidney (HEK) 293T cells transfected with wild-type cathD (*cathD^wt*) or catalytically inactive cathD (*cathD^D231N*) fused with a c-myc tag were treated with the Hsp70 inhibitor or control HBSS for 24 hours. Total proteins from different groups were subjected to immunoblot analysis. GAPDH, glyceraldehyde-3-phosphate dehydrogenase. **(H)** Quantifications of normalized p-cofilin/total cofilin ratio obtained from Western blots in (G). Note a significant decrease in p-cofilin levels in both *cathD^wt* and *cathD^D231N* cells upon HSP inhibitor I treatment. Data are shown as means ± SEM. ***$P < 0.001$ by one-way ANOVA with Newman-Keuls multiple comparison test among three groups or above.

In addition, enhanced green fluorescent protein (EGFP)–fused cathD exhibited a periphery distribution at lamellipodia in HeLa cells treated with HSP inhibitor I that enhances potential cytosolic translocation (Fig. 4F). Human embryonic kidney (HEK) 293T cell line transfected with wild-type *cathD* (*cathD^wt*) or proteolytically inactive *cathD* (*cathD^D231N*) was treated with HSP inhibitor I to investigate whether cathD regulates cofilin activation via its proteolytic activity. HSP inhibitor I treatment reduced p-cofilin levels in both *cathD^wt* and *cathD^D231N* cells (Fig. 4, G and H), suggesting that cytosolic cathD regulates cofilin phosphorylation levels independent of its proteolytic activity.

CathD regulates cell motility by enhancing actin turnover

During cell migration, coordinated actin dynamics generate protrusive force to constantly push the leading edge forward (*24*). To further investigate how cathD regulates actin dynamics, microglia were treated with jasplakinolide (JAS), a drug that stabilizes actin filaments by competing with cofilin for actin binding (*28, 29*). JAS treatment disrupted lamellipodia extension, a phenotype resembling the lamellipodia extension defects in *cathD*-deficient microglia, and failed to rescue these defects in the absence of cathD (Fig. 5, A to D, and movies S6 and S7). Moreover, in *cathD*-deficient microglia, none of the retraction parameters changed after JAS treatment (fig. S3, A to C).
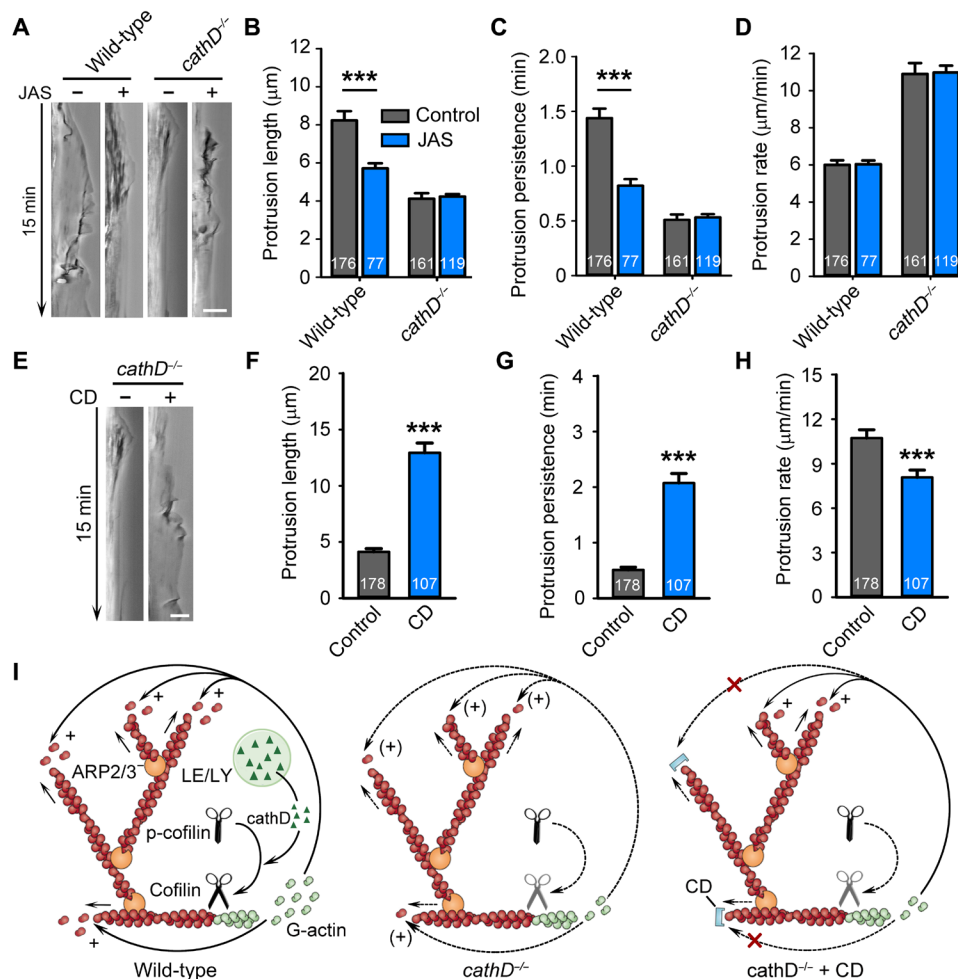
Fig. 5. CathD coordinates leading edge dynamics by replenishing local G-actin pool. (**A**) Representative kymograph images showing that jasplakinolide (JAS) inhibits ATP-γ-S–induced lamellipodia maintenance in wild-type microglia but does not affect *cathD*-deficient (*cathD*$^{-/-}$) microglia. (**B** to **D**) Quantifications of protrusion length (B), persistence (C), and rate (D) obtained from 232 to 292 events in a minimum of 77 cells per group. (**E** to **H**) Representative kymograph images (E) and quantifications (F to H) of membrane protrusions from *cathD*-deficient microglia preincubated with or without cytochalasin D (CD; 25 nM), showing that CD rescues maintenance failure of lamellipodia in *cathD*-deficient microglia during ATP-γ-S stimulation. Quantifications of protrusion length (F), persistence (G), and rate (H) obtained from 320 to 533 events in a minimum of 107 cells per group. (**I**) Schematic diagrams illustrating the mechanism of cathD in regulating actin reorganization via recycling G-actin. LE/LY, late endosome/lysosomes. Data are shown as means ± SEM. ***$P < 0.001$ by unpaired Student's *t* test or one-way ANOVA with Newman-Keuls multiple comparison test among three groups or above.

These results rule out the possibility that cathD depletion induces overdepolymerization of actin filaments.

To determine whether actin incorporation is affected by the absence of cathD, *cathD*-deficient microglia were pretreated with low-dose cytochalasin D (CD; 25 nM), which caps a limited number of barbed ends so that G-actin can be efficiently used for growth of uncapped filaments (*30*). CD rescued the lamellipodia extension defects in *cathD*-deficient microglia by increasing the protrusion length and persistence but only slightly affected protrusion rate and retraction parameters as shown by kymograph analysis (Fig. 5, E to H; fig. S3, D to F; and movie S8). To further confirm the regulatory role of cathD in actin dynamics, we applied an in vitro actin depolymerization assay and found that both cathD^{wt} and proteolytically inactive cathD^{D231N} facilitated cofilin-based actin filaments severing (fig. S4, A and B), suggesting that cathD nonproteolytically promotes cofilin-mediated actin turnover.

In toto, these results indicate that cathD modulates actin remodeling by enhancing actin turnover. In the absence of cathD, the

G-actin pool is initially sufficient for actin filament assembly, ensuring the first waves of lamellipodia formation. Subsequently, however, cofilin hyperphosphorylation abolishes its severing activity and decreases the local G-actin pool for reassembly, leading to insufficient actin polymerization and consequent failure in lamellipodia maintenance. After partially capping barbed ends, other uncapped filaments are incorporated with limited amount of G-actin and polymerization resumes (Fig. 5I).

CathD mediates directional migration of microglia

To further examine the potential role of cathD for microglia motility in vivo, injury-induced migration was examined in real time using neonatal *CX3CR1*$^{+/GFP}$ and *CX3CR1*$^{+/GFP}$;*cathD*$^{-/-}$ mice on postnatal day 15, before brain damage occurs (*31*). Upon laser injury, rapid microglia migration was induced in the neocortical region of *CX3CR1*$^{+/GFP}$ mice (Fig. 6A). Notably, microglia dynamics were significantly impaired in *CX3CR1*$^{+/GFP}$;*cathD*$^{-/-}$ mice (Fig. 6B and movies S9 and S10). Consistent with the in vivo data, local injection
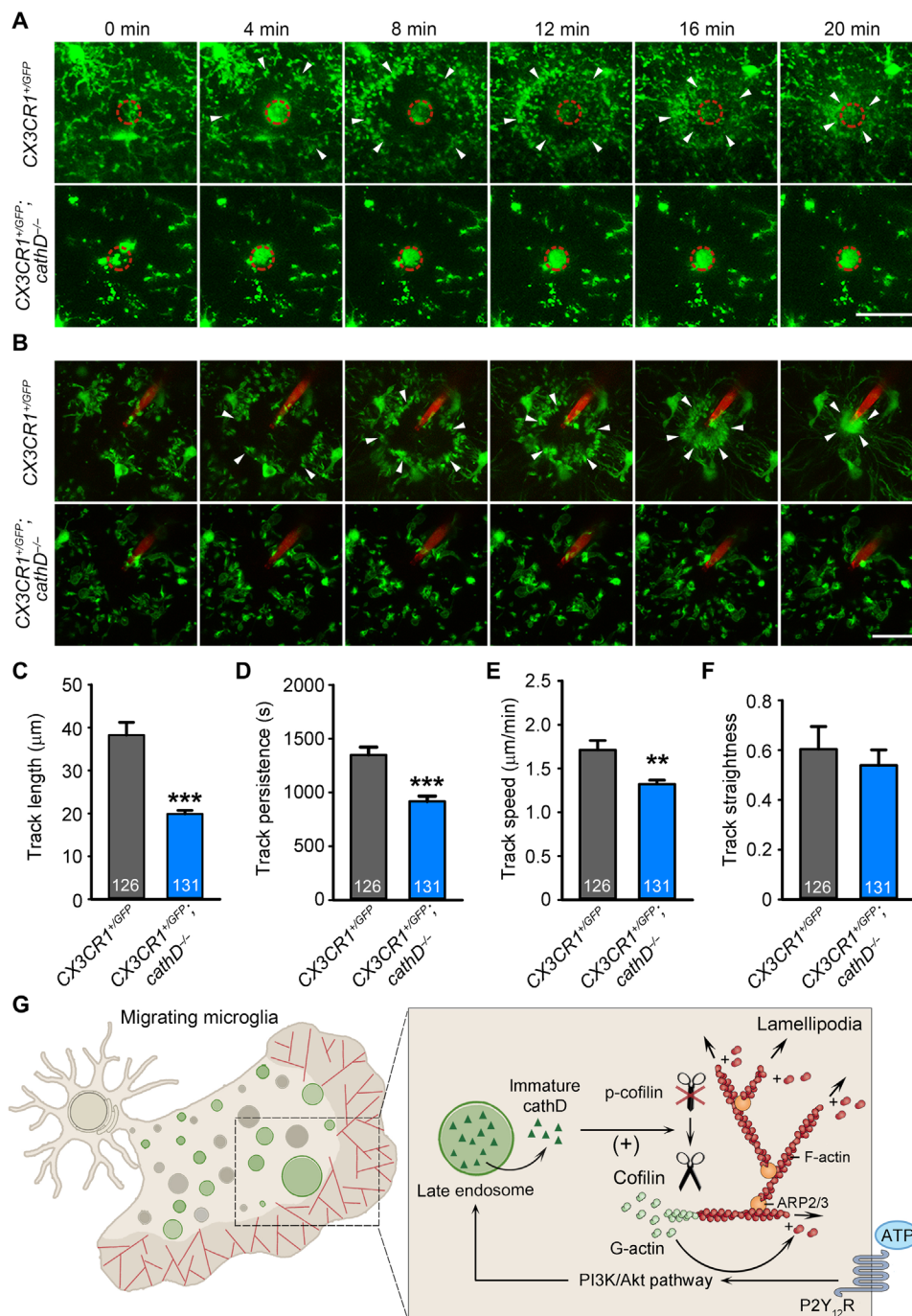
Fig. 6. CathD mediates directional migration of microglia in vivo. (**A**) Time-lapse analysis of cortical microglia migration in P15 $CX3CR1^{+/GFP}$ and $CX3CR1^{+/GFP};cathD^{-/-}$ mice in vivo. Live images were captured by two-photon microscopy every 4 min after the 860-nm laser injury. The red circle indicates the injury site. Note a rapid protrusion extension toward the injury site in wild-type microglia. This migration was absent in $cathD$ KO microglia. Scale bar, 40 μm. (**B**) Time-lapse analysis of microglia migration in P15 $CX3CR1^{+/GFP}$ and $CX3CR1^{+/GFP};cathD^{-/-}$ mice brain slices. Microglia migration was induced by a micropipette filled with 5 mM ATP and 10 mM Alexa Fluor 594 in artificial cerebrospinal fluid (ACSF). Scale bar, 40 μm. (**C** to **F**) Quantifications of tracking parameters for microglial protrusions in the brain. A decrease in length (C), persistence (D), and speed (E) was detected in $CX3CR1^{+/GFP};cathD^{-/-}$ mice brain slices. Track direction (F) remains similar between groups. Data are shown as means ± SEM. $**P < 0.01$ and $***P < 0.001$ by unpaired Student's t test. (**G**) A schematic model for the role of immature 48-kDa cathD in regulating actin dynamics in microglia. During ATP signaling–induced microglia migration, the PI3K pathway activated by $P2Y_{12}$ receptors ($P2Y_{12}$Rs) increases the membrane permeability of late endosomes and triggers cytosolic translocation of the immature 48-kD cathD. Translocated cathD regulates actin cytoskeleton remodeling by balancing cofilin activity to recycle local G-actin monomers for consequent lamellipodia extension and cell migration.

of ATP in *CX3CR1*^{+/GFP} brain slices evoked extensive microglial responses, whereas very limited number of *CX3CR1*^{+/GFP}*;cathD*^{−/−} microglia extended their processes to the ATP injection site (Fig. 6B, fig. S3G, and movies S11 and 12). Our tracking analysis showed that cathD depletion decreased the protrusion length, persistence, and speed (Fig. 6, C to E). In comparison, the direction and the speed variation of these processes remained comparable between groups (Fig. 6F and fig. S3H). To confirm the role of cathD in microglia migration, we next analyzed the directional migration of microglia using an in vitro micropipette assay that mimics endogenous ATP release during injury (*18*, *32*). Compared with wild-type controls, cathD-deficient microglia exhibited a suppressed migration activity upon ATP-γ-S stimulation (fig. S5A and movies S13 and 14), as shown by a decreased migration rate and track length (fig. S5, B and C).

Considering that enhancing potential cytosolic translocation evoked lamellipodia-distribution of cathD (Fig. 4F) and increased cofilin activity (Fig. 4, G and H), we performed a wound-healing assay to examine whether cytosolic translocation of cathD could promote tumor cell migration. We established a cathD-deficient (cathD^{−/−}) HeLa cell line using a lentivirus-based CRISPR-Cas9 system and then re-introduced cathD or its proteolytically inactive mutant cathD^{D231N} into this cathD^{−/−} cell line. We found that depletion of cathD reduced the migration ability of HeLa cells as shown by a decreased wound healing rate, which could be restored by both cathD^{wt} and cathD^{D231N} (fig. S5, D and E). These results suggest that cathD also nonproteolytically promotes migration in tumor cells. However, enhancing potential cytosolic translocation by HSP inhibitor I did not affect the wound healing activity in either cathD^{wt}- or cathD^{D231N}-reintroduced cells (fig. S5, D and E), implying that other factors, such as adhesion and proliferation molecules, might also be crucial for tumor invasion. Together with above results, we conclude that cytosolically translocated cathD regulates cofilin-driven actin remodeling, which, in turn, promotes lamellipodial extension and facilitates ATP-evoked microglia migration (Fig. 6G).

DISCUSSION

In the present study, we demonstrate that late endosome–derived immature hydrolase cathD promotes cytoskeleton remodeling after its cytosolic translocation. Cytosolically translocated cathD balances the activity of the actin-severing protein cofilin to maintain lamellipodia extension in ATP-mediated microglial responses by replenishing G-actin pool during fast cell migration. Among different forms during maturation, late endosome–derived 48-kDa immature cathD is uniquely translocated to the cytosol and colocalizes with actin cytoskeleton at the leading edge during ATP-evoked microglia migration. Gene depletion or inhibition of cytosolic translocation of cathD markedly impairs lamellipodia maintenance, indicating that cytosolically translocated cathD contributes to actin remodeling. Our results highlight late endosomes as novel modulators of actin dynamics and lamellipodia extension via cytosolic translocation of cathD.

Cathepsins degrade extracellular matrix after extracellular secretion or activate other extracellular enzymes to initiate "outside-in" signal cascades to promote cell migration (*33*, *34*). However, cathD is the only lysosomal protease that translocates to the cytosol upon ATP treatment in our observation, indicative of a unique role of cathD in regulating fast microglia migration. Outside acidic endosomal/lysosomal vesicles, cathD has also been widely detected in the cytosol, extracellular space, and even the nuclear region, where the pH

is far beyond the optimal range for its canonical proteolysis function (*35*, *36*). Accumulating evidence shows that inactive cathD non-proteolytically promotes cell migration, proliferation, and apoptosis (*37*–*39*). In this study, we provide evidence that the cytosolically translocated immature cathD promotes cofilin dephosphorylation without degrading cofilin, pointing to a nonproteolytic role of immature cathD in regulating actin remodeling. Transfection of proteolytically inactive cathD, as well as wild-type cathD, reduces p-cofilin levels in cell lines, indicating that cathD modulates cofilin activity independent on its proteolytic activity. In our view, these findings indicate a functional expansion of cathD outside the endosomal/lysosomal vesicles before its maturation and make a strong case for a noncanonical role of late endosomes in controlling cyto-skeleton dynamics. During lamellipodia extension, actin cytoskeleton undergoes constant remodeling by recycling G-actin through multiple steps (*31*, *40*). To reveal the steps regulated by cathD, cathD-deficient microglia are treated with JAS to prevent actin de-polymerization or low dose of CD to partially inhibit polymeriza-tion. In our observation, JAS fails to revert the reduced lamellipodia dynamics, ruling out the possibility of overdepolymerization. In comparison, lamellipodia maintenance defects in cathD-deficient microglia are rescued in the presence of CD, which caps a limited number of barbed ends and allows an economical use of regenerated G-actin to support the growth of uncapped filaments (*30*). These results indicate that cathD modulates actin remodeling by controlling G-actin monomer recycling. In the absence of cathD, the G-actin pool is initially sufficient for actin filament assembly, ensuring the first waves of lamellipodia formation. Later on, however, cofilin hyperphosphorylation abolishes its severing activity and decreases the local G-actin pool for reassembly, leading to insufficient actin polymerization and consequent failure in lamellipodia persistence.

The mechanism of cathD cytosolic translocation remains to be explored. Although we reveal that impaired endosomal/lysosomal integrity is responsible for cathD cytosolic translocation, the involve-ment of other factors such as transporters or channels cannot be ruled out. Notably, cathD is present on the endosomal/lysosomal membrane of macrophage, suggestive of a membrane-inserted or transmembrane state of cathD (*41*). Through this line, acid sphingomyelinase–derived ceramide has been implicated in recruit-ing cathD to the endosome membrane (*41*, *42*). In addition, several candidate transporters at the endosomal/lysosomal membrane have been identified. For example, LAMP2A in the multimeric state has been shown to act as channels for substrate delivery crossing the endosomal/lysosomal membrane in chaperone-mediated autophagy (*43*). Intriguingly, cathD contains five KFERQ-like motifs in its heavy-chain region (*44*), which are required for transport across the endosomal/lysosomal membrane through LAMP2A channels but rarely seen in organelle proteins. These motifs may also make cathD a unique lysosomal protease that can translocate to the cyto-sol and regulate actin dynamics. Future investigations will help to elucidate the detailed mechanism and identify additional players of cathD cytosolic translocation.

In conclusion, our findings demonstrate that late endosome-derived cathD promotes actin-driven lamellipodial extension in ATP-evoked microglia migration. Cytosolic cathD balances cofilin activity and modulates G-actin pool in actin cytoskeleton remodeling. In addition, both cathD^{wt} and its proteolytically inactive mutant promote actin disassembly. These findings may shed light on the proteolysis-independent role of cathD in promoting cytoskeleton

remodeling, which is used by late endosomes to regulate fast cell migration. Future studies are needed to investigate the mechanisms underlying cathD-modulated cofilin phosphorylation and actin cytoskeleton remodeling. Moreover, our study implicates a non-canonical activity of immature cathD in neutral pH cytosol, which may modulate other relevant cellular processes via regulating cofilin activity.

MATERIALS AND METHODS

General reagents and antibodies
Commercial reagents and antibodies were obtained from Cell Signaling Technology (cofilin, pLIMK1/2, EEA1, p-Akt, and Akt), R&D Systems (cathD), Sigma-Aldrich (glyceraldehyde-3-phosphate dehydrogenase, β-actin, and α-tubulin), Santa Cruz Biotechnology (p-cofilin, cathB, cathD, cathL, and cathE), Developmental Studies Hybridoma Bank (DSHB and LAMP2), Enzo Life Sciences (LAMP1 and rHsp70), Life Technologies (Alexa Fluor 488–conjugated secondary antibodies, Alexa Fluor 555/Rhodamine–conjugated phalloidin, AM1-43, CM-DiI, LysoTracker, AO, and JAS), Jackson ImmunoResearch (Cy3, Cy5, and horseradish peroxidase–conjugated secondary antibodies), and Roche (proteases and phosphatase inhibitor cocktails). See summary of antibodies and dyes used in experiments in table S1. All other reagents were from Sigma-Aldrich. Cells were obtained from American Type Culture Collection.

Animals
The use and care of animals are in compliance with the guidelines of the Institutional Animal Care and Use Committee. *Rab27a*-deficient mice (C3H/HeSn-*Rab27aash/J*) were obtained from the Jackson laboratory (Bar Harbor, ME). *CathD*-deficient mice were gifts from P. Saftig (Institute of Biochemistry, Christian-Albrechts-Universität Kiel, Germany).

Cell culture and transfection
Primary microglia were cultured as described previously (*18*). Briefly, cerebral cortex was dissociated from neonatal Sprague-Dawley rat brains and digested with 0.25% trypsin. The mixture was plated on flasks precoated with poly-D-lysine and maintained for 7 to 10 days in minimum essential medium (MEM) with 10% fetal bovine serum (FBS). Microglia were separated from mixed glial culture by gentle shaking, transferred to appropriate glass coverslips or dishes without coating, and maintained in low-FBS medium (3% FBS in MEM) for 4 to 8 hours before experiments. Primary microglia were prepared from *cathD*- or *Rab27a*-deficient mice. BV2 cells were cultured in Dulbecco's MEM (DMEM) supplemented with 10% FBS. Transient transfections were performed using Lipofectamine 2000 for BV2 cells, Turbofect for HeLa and HEK293T cells, and Oligofectamine for primary microglia. The small interfering RNA (siRNA) sequence 5′-GGGTTCTCTGTCCTACCTG-3′ was designed against rat *cathD* and synthesized by Thermo Fisher Scientific. The efficiency of cathD knockdown sequence was applied by Western blot before use (fig. S6, A to C).

Single-cell tracking and kymograph analysis
Lamellipodia dynamics were analyzed by single-cell tracing analysis. Primary microglia treated with 10 μM ATP-γ-S were pretreated with rHsp70 (300 nM), JAS (15 nM), or CD (25 nM). For kymograph analysis, images were captured using confocal microscopy with a 40× 0.6 numerical aperture (NA) objective in phase contrast mode at 1-s intervals. More than six videos were captured and processed by the ImageJ software for each independent experiment. A custom-made perl script was used to calculate lamellipodia parameters such as extension rate, duration, and distance.

Immunohistochemistry
Primary microglia plated on coverslips were fixed with 4% paraformaldehyde in phosphate-buffered saline (PBS) at room temperature for 10 min and permeabilized with 0.1% Triton X-100 in PBS or pure methanol (−20°C) for 5 to 10 min. After blocking with 10% bovine serum albumin for 1 hour at room temperature, cells were then incubated with primary antibodies against LAMP1 (1:200), EEA1 (1:500), cathD (1:200), cofilin (1:200), p-cofilin (1:200), or α-tubulin (1:500) overnight at 4°C. Note that the specificity of the cathD antibody was verified by Western blot and immunostaining (fig. S6, B and C). After incubation, cells were washed and incubated for 1 hour at room temperature with the fluorescence-conjugated secondary antibodies (Alexa Fluor 488, Cy3 and/or Cy5-donkey anti-rabbit, anti-goat, or anti-mouse; 1:1000). F-actin was labeled with phalloidin conjugated with Alexa Fluor 555 or Rhodamine (1:200) for 2 hours at room temperature. Nucleus counterstaining was performed with 4′,6-diamidino-2-phenylindole (DAPI). For dye staining, microglia were loaded with AM1-43 (10 μM) overnight or LysoTracker (1:20,000) 5 min and rinsed slightly once with warm Hank's balanced salt solution (HBSS) before ATP-γ-S treatment and fixation. Images were captured by Olympus confocal microscope (FV 1000), Nikon confocal microscope (Nikon A1R), or ZEISS superresolution structured illumination microscope (ELYRA S.1). For colocalization analysis, images were imported to the ImageJ software, and Pearson's *r* coefficient was determined by the Coloc2 plugin. Pearson's *r* values were presented as means ± SEM.

Co-IP and Western blotting analysis
Cell lysates were prepared in the cold lysis buffer [20 mM tris (pH 7.5), 150 mM NaCl, and 1% Triton X-100]. After being precleaned with normal goat immunoglobulin G, cell lysates (0.5 to 1 mg of protein in a final volume of 0.5 ml) were incubated with primary antibodies (3 to 5 μg) overnight and subsequently with 20 μl of protein A/G agarose beads. Immunoprecipitated proteins were collected, washed with the radioimmunoprecipitation assay buffer three times, separated by SDS–polyacrylamide gel electrophoresis (PAGE), and transferred to a PVDF membrane for Western blotting. For Fourier-transform ion cyclotron resonance mass spectrometry (LC-ESI-LTQ-FTICR-MS), the immune complexes were separated by incubation in 8 M urea for 30 min and centrifuged at 2000*g* for 2 min.

Lysosomal integrity analysis
To analyze lysosomal integrity, we used a real-time imaging protocol of cells stained with AO (*25*). Primary microglia were incubated with AO (2 μg/ml) for 15 min at 37°C and rinsed with HBSS with 3% FBS. Cells from random areas were visualized and exposed to blue light for 20 s. Subsequently, images were captured for 10 min at 20-s intervals. By measuring the red color intensities, changes in lysosomal pH gradient were quantified.

Preparation of S100 fractions from primary microglia
After washed once with ice-cold HBSS, ATP-γ-S–treated primary microglia and their controls were removed from 100-mm dishes

with a hypotonic buffer [20 mM Hepes-KOH (pH 7.5), 10 mM KCl, 2 mM EDTA, 0.25 M sucrose, and 1 mM dithiothreitol (DTT)] supplemented with protease inhibitor cocktails. Following incubation on ice for 15 min, cells were disrupted by douncing 15 times in a Dounce homogenizer. Debris and unbroken cells were first removed after 1000g for 6 min at 4°C. The supernatant (S1) was centrifuged again at 10,000g for 1 hour to remove cell organelles. The supernatant (S2) was further centrifuged at 100,000g for 1 hour in a Beckman SW28 rotor. The resulting supernatant (S100 fraction) was then analyzed with Western blotting.

G-actin/F-actin pool fraction

To separate Triton X-100–soluble G-actin and insoluble F-actin, lysis and F-actin stabilization buffer (LAS1) was prepared with the following components: 50 mM Pipes (pH 6.9), 50 mM NaCl, 5 mM MgCl$_2$, 5 mM EGTA, 5% (v/v) glycerol, 0.1% NP-40, 0.1% Triton X-100, 0.1% Tween-20, 0.1% 2-mercaptoethanol, and 0.001% Antifoam C. Cells were removed with scrapers with appropriate volume of warm LAS2 (2 ml of LAS1 buffer, 20 μl of 100 mM ATP, and 20 μl of protease inhibitor cocktails). Using a 25-gauge syringe, cells were homogenized and incubated at 37°C for 10 min. One-hundred microliters of lysates was centrifuged at 350g at room temperature for 5 min to pellet the unbroken cells. Supernatants were pipetted into clearly labeled ultracentrifuge tubes and centrifuged at 100,000g at room temperature for 1 hour to pellet F-actin (G-actin was in the supernatant). F-actin pellet was depolymerized by 100 nM CD in PBS.

Live imaging of GFP-labeled microglia migration

For the intravital imaging, P15 $CX3CR1^{+/GFP}$ and $CX3CR1^{+/GFP}$; $cathD^{-/-}$ mice were anesthetized with intraperitoneal injections of pentobarbital sodium (50 mg/kg) on warm plates. Thinned skull intravital window surgeries and laser ablation were performed as previously described (16). Live imaging and laser injury were conducted with an Olympus two-photon microscope. Using a 40× 0.8 NA water dipping objective, stacks of images were acquired with a step size of 1 μm on the mouse cortex with a depth of 100 to 200 μm below the skull. Laser injury was induced by Ti:Sapphire laser (Mai-Tai, Spectra-Physics) for 15 μm in diameter. Time-lapse videos were then generated at 2-min intervals between three-dimensional stacks for 30 min.

Brain slices were prepared from P15 $CX3CR1$-GFP heterozygous mice with a thickness of 300 μm. Micropipette with a tip opening of ~2 μm was filled with 5 mM ATP and 10 mM Alexa Fluor 594 dye. The tip of pipette was placed in the center of imaging region, and stacks of images were captured using a 40× water dipping objective with a step size of 1 μm. Live images were generated for 30 min at 2-min intervals with an upright confocal microscope (Olympus, FV 1000).

Micropipette-based migration assay

To investigate the motility of primary microglia, we applied an in vitro micropipette-based system to analyze the directional migration of microglia as detailed previously (18, 32). Briefly, a chemotactic gradient was created by pulsatile injection of ATP-γ-S (1 mM) through a micropipette to trigger microglia migration using an electrically gated pressure application system (Picosprizer II, Parker Co.). Live images were captured for 30 min at 2-min intervals using a microscope (Olympus, FV 1200) with a 20× air objective (LCACH, 0.4 NA). Migration tracks were analyzed from migrating microglia

that were 150 to 250 μm away from the pipette tip by the ImageJ software.

Lentivirus-based gene editing and stable cell line establishment

Single guide RNA (sgRNA)–encoding oligonucleotides were designed, synthesized, and cloned into LentiCRISPRv2-GFP lentiviral vector to express Cas9, GFP, and sgRNA-targeting cathD. Subsequently, LentiCRISPRv2-cathD sgRNA-GFP or its control LentiCRISPRv2-GFP vector were transfected along with psPAX2 packaging plasmid and pMD2.G envelope plasmid into Lenti-X 293T cells at a ratio of 4:3:1. Transfected cells were cultured in DMEM with high glucose (4.5 g/liter) supplemented with 20% FBS for 48 hours. Lentiviral particles were then collected by centrifugation at 10,000g from the harvested medium and diluted with DMEM plus 10% FBS (1:1 in volume) with 10 μM polybrene (Sigma-Aldrich) before being added to HeLa cells.

To establish stable cathD-deficient (cathD$^{-/-}$) HeLa cell lines, GFP-positive HeLa cells were sorted using MoFlo Astrios EQ cell sorter (Beckman, Brea, CA) after 36 to 48 hours of lentiviral transduction. The cathD knockout of cathD was validated by Western blot (fig. S6D). To further reintroduce wild-type human cathD (cathD^{wt}) or its proteolytically inactive mutant cathD^{D231N}, pLVX-Puro-cathD^{wt}, and pLVX-Puro-cathD^{D231N} constructions were packaged into viral particles and transfected into cathD$^{-/-}$ HeLa cells. At 48 hours after transduction, puromycin (Clontech) was added to the culture medium to a final concentration of 3 μg/ml for establishing stable cell lines. For protein purification, we generated stably transfected HEK293T cell lines using similar strategies to prevent protein aggregation and the formation of insoluble inclusion bodies. Using a standardized protocol, recombinant human cathD^{wt}, cathD^{D231N}, and cofilin with a 6× His-tag were purified and stored at −80°C in 150 mM NaCl (pH 7.4), 0.05% sodium azide, and 25% glycerol before subsequent experiments. For quality control, purified proteins were checked by silver staining following SDS-PAGE separation (fig. S6, E to G).

In vitro wound-healing and migration assay

HeLa cells carrying different cathD mutants were cultured in μ-Dish$^{35\,mm}$ with inserts (ibid, Munich, Germany) at a density of 5×10^4 cells per well until monolayers were confluent. In the presence or absence of HSP inhibitor I (15 μM) or control HBSS, cells were cultured in low-FBS medium (2% FBS in MEM) to suppress proliferation. Inserts were then removed to create a cell-free gap of 500 μm after cells reach confluence, allowing cells to migrate for wound healing. Images were then captured at different time points using a phase-contrast microscope. The migration ability was analyzed by measuring wound area closure at each time point by the ImageJ software.

In vitro actin depolymerization assay

The actin filament severing was examined as previously described (40, 45). Briefly, rhodamine-labeled actin monomers (5 μM) were polymerized to filaments at room temperature in F buffer [10 mM tris-HCl (pH 7.5), 0.2 mM CaCl$_2$, 50 mM KCl, 2 mM MgCl$_2$, 0.5% methylcellulose, 0.2 mM DTT, and 0.7 mM ATP] for 1 hour. To initiate actin depolymerization, preassembled actin filaments were mixed with MKEI-50 buffer [20 mM imidazole (pH 7.0), 50 mM KCl, 2 mM MgCl$_2$, 1 mM EGTA, and 0.5 mM DTT] to a final concentration 0.1 μM and then added with purified cathD^{wt} or proteolytically

inactive cathD^{D231N} (500 nM), with or without cofilin (300 nM). Mixed actin filaments were added on 0.1% nitrocellulose–coated coverslips (50 mm by 5 mm) and observed by a confocal microscope with a 60× water-immersion, 1.2-NA objective at indicated time points.

Statistical analysis

Statistical analysis was performed by one-way analysis of variance (ANOVA) (followed by Newman-Keuls multiple comparison test) and unpaired Student's *t* test. All data were tested for the comparability of their variances using an *F* test. Data were presented as means ± SEM. *P* < 0.05 was considered statistically significant. See summary of statistical methods and results in table S2.

SUPPLEMENTARY MATERIALS

Supplementary material for this article is available at http://advances.sciencemag.org/cgi/content/full/6/50/eaba5783/DC1

View/request a protocol for this paper from *Bio-protocol*.

REFERENCES AND NOTES

1. S. Aits, M. Jäättelä, Lysosomal cell death at a glance. *J. Cell Sci.* **126**, 1905–1912 (2013).
2. B. Turk, V. Turk, Lysosomes as "suicide bags" in cell death: Myth or reality? *J. Biol. Chem.* **284**, 21783–21787 (2009).
3. M. L. Skowyra, P. H. Schlesinger, T. V. Naismith, P. I. Hanson, Triggered recruitment of ESCRT machinery promotes endolysosomal repair. *Science* **360**, eaar5078 (2018).
4. M. Radulovic, K. O. Schink, E. M. Wenzel, V. Nähse, A. Bongiovanni, F. Lafont, H. Stenmark, ESCRT-mediated lysosome repair precedes lysophagy and promotes cell survival. *EMBO J.* **37**, e99753 (2018).
5. Z. Jevnikar, N. Obermajer, M. Bogyo, J. Kos, The role of cathepsin X in the migration and invasiveness of T lymphocytes. *J. Cell Sci.* **121**, 2652–2661 (2008).
6. J. Kos, Z. Jevnikar, N. Obermajer, The role of cathepsin X in cell signaling. *Cell Adh. Migr.* **3**, 164–166 (2009).
7. S. Koch, E. Scifo, A. Rokka, P. Trippner, M. Lindfors, R. Korhonen, G. L. Corthals, I. Virtanen, M. Lalowski, J. Tyynelä, Cathepsin D deficiency induces cytoskeletal changes and affects cell migration pathways in the brain. *Neurobiol. Dis.* **50**, 107–119 (2013).
8. A. Latifkar, L. Ling, A. Hingorani, E. Johansen, A. Clement, X. Zhang, J. Hartman, C. Fischbach, H. Lin, R. A. Cerione, M. A. Antonyak, Loss of sirtuin 1 alters the secretome of breast cancer cells by impairing lysosomal integrity. *Dev. Cell* **49**, 393–408.e7 (2019).
9. J. T. Parsons, A. R. Horwitz, M. A. Schwartz, Cell adhesion: Integrating cytoskeletal dynamics and cellular tension. *Nat. Rev. Mol. Cell Biol.* **11**, 633–643 (2010).
10. Y.-J. Liu, M. L. Berre, F. Lautenschlaeger, P. Maiuri, A. Callan-Jones, M. Heuzé, T. Takaki, R. Voituriez, M. Piel, Confinement and low adhesion induce fast amoeboid migration of slow mesenchymal cells. *Cell* **160**, 659–672 (2015).
11. M. Bergert, S. D. Chandradoss, R. A. Desai, E. Paluch, Cell mechanics control rapid transitions between blebs and lamellipodia during migration. *Proc. Natl. Acad. Sci. U.S.A.* **109**, 14434–14439 (2012).
12. L. Delamarre, M. Pack, H. Chang, I. Mellman, E. S. Trombetta, Differential lysosomal proteolysis in antigen-presenting cells determines antigen fate. *Science* **307**, 1630–1634 (2005).
13. S. E. Haynes, G. Hollopeter, G. Yang, D. Kurpius, M. E. Dailey, W.-B. Gan, D. Julius, The P2Y$_{12}$ receptor regulates microglial activation by extracellular nucleotides. *Nat. Neurosci.* **9**, 1512–1519 (2006).
14. S. Honda, Y. Sasaki, K. Ohsawa, Y. Imai, Y. Nakamura, K. Inoue, S. Kohsaka, Extracellular ATP or ADP induce chemotaxis of cultured microglia through G$_{i/o}$-coupled P2Y receptors. *J. Neurosci.* **21**, 1975–1982 (2001).
15. T. Nagano, S. H. Kimura, M. Takemura, Prostaglandin E$_2$ reduces extracellular ATP-induced migration in cultured rat microglia. *Brain Res.* **1221**, 1–5 (2008).
16. D. Davalos, J. Grutzendler, G. Yang, J. V. Kim, Y. Zuo, S. Jung, D. R. Littman, M. L. Dustin, W.-B. Gan, ATP mediates rapid microglial response to local brain injury in vivo. *Nat. Neurosci.* **8**, 752–758 (2005).
17. J. A. Swanson, Shaping cups into phagosomes and macropinosomes. *Nat. Rev. Mol. Cell Biol.* **9**, 639–649 (2008).
18. Y. Dou, H.-j. Wu, H.-q. Li, S. Qin, Y.-e. Wang, J. Li, H.-f. Lou, Z. Chen, X.-m. Li, Q.-m. Luo, S. Duan, Microglial migration mediated by ATP-induced ATP release from lysosomes. *Cell Res.* **22**, 1022–1033 (2012).
19. M. Ostrowski, N. B. Carmo, S. Krumeich, I. Fanget, G. Raposo, A. Savina, C. F. Moita, K. Schauer, A. N. Hume, R. P. Freitas, B. Goud, P. Benaroch, N. Hacohen, M. Fukuda, C. Desnos, M. C. Seabra, F. Darchen, S. Amigorena, L. F. Moita, C. Thery, Rab27a

20. and Rab27b control different steps of the exosome secretion pathway. *Nat. Cell Biol.* **12**, 19–30 (2010).
21. T. Tolmachova, R. Anders, J. Stinchcombe, G. Bossi, G. M. Griffiths, C. Huxley, M. C. Seabra, A general role for Rab27a in secretory cells. *Mol. Biol. Cell* **15**, 332–344 (2004).
22. S. M. Wilson, R. Yip, D. A. Swing, T. N. O'Sullivan, Y. Zhang, E. K. Novak, R. T. Swank, L. B. Russell, N. G. Copeland, N. A. Jenkins, A mutation in Rab27a causes the vesicle transport defects observed in ashen mice. *Proc. Natl. Acad. Sci. U.S.A.* **97**, 7933–7938 (2000).
23. L. A. Ginsel, J. J. Onderwater, J. A. Fransen, A. J. Verhoeven, D. Roos, Localization of the low-Mr subunit of cytochrome b558 in human blood phagocytes by immunoelectron microscopy. *Blood* **76**, 2105–2116 (1990).
24. N. Zaidi, A. Maurer, S. Nieke, H. Kalbacher, Cathepsin D: A cellular roadmap. *Biochem. Biophys. Res. Commun.* **376**, 5–9 (2008).
25. A. Nürnberg, T. Kitzing, R. Grosse, Nucleating actin for invasion. *Nat. Rev. Cancer* **11**, 177–187 (2011).
26. T. Kirkegaard, A. G. Roth, N. H. T. Petersen, A. K. Mahalka, O. D. Olsen, I. Moilanen, A. Zylicz, J. Knudsen, K. Sandhoff, C. Arenz, P. K. J. Kinnunen, J. Nylandsted, M. Jäättelä, Hsp70 stabilizes lysosomes and reverts Niemann–Pick disease-associated lysosomal pathology. *Nature* **463**, 549–553 (2010).
27. J. Nylandsted, M. Gyrd-Hansen, A. Danielewicz, N. Fehrenbacher, U. Lademann, M. Høyer-Hansen, E. Weber, G. Multhoff, M. Rohde, M. Jäättelä, Heat shock protein 70 promotes cell survival by inhibiting lysosomal membrane permeabilization. *J. Exp. Med.* **200**, 425–435 (2004).
28. J. R. Bamburg, O. P. Wiggan, ADF/cofilin and actin dynamics in disease. *Trends Cell Biol.* **12**, 598–605 (2002).
29. M. R. Bubb, I. Spector, B. B. Beyer, K. M. Fosen, Effects of jasplakinolide on the kinetics of actin polymerization. An explanation for certain in vivo observations. *J. Biol. Chem.* **275**, 5163–5170 (2000).
30. E. Jovceva, M. R. Larsen, M. D. Waterfield, B. Baum, J. F. Timms, Dynamic cofilin phosphorylation in the control of lamellipodial actin homeostasis. *J. Cell Sci.* **120**, 1888–1897 (2007).
31. J. E. Bear, T. M. Svitkina, M. Krause, D. A. Schafer, J. J. Loureiro, G. A. Strasser, I. V. Maly, O. Y. Chaga, J. A. Cooper, G. G. Borisy, F. B. Gertler, Antagonism between Ena/VASP proteins and actin filament capping regulates fibroblast motility. *Cell* **109**, 509–521 (2002).
32. P. Saftig, M. Hetman, W. Schmahl, K. Weber, L. Heine, H. Mossmann, A. Köster, B. Hess, M. Evers, K. von Figura, Mice deficient for the lysosomal proteinase cathepsin D exhibit progressive atrophy of the intestinal mucosa and profound destruction of lymphoid cells. *EMBO J.* **14**, 3599–3608 (1995).
33. H.-j. Wu, Y.-j. Liu, H.-q. Li, C. Chen, Y. Dou, H.-f. Lou, M. S. Ho, X.-m. Li, Z. Gao, S. Duan, Analysis of microglial migration by a micropipette assay. *Nat. Protoc.* **9**, 491–500 (2014).
34. M. M. Mohamed, B. F. Sloane, Cysteine cathepsins: Multifunctional enzymes in cancer. *Nat. Rev. Cancer* **6**, 764–775 (2006).
35. V. Gocheva, J. A. Joyce, Cysteine cathepsins and the cutting edge of cancer invasion. *Cell Cycle* **6**, 60–64 (2007).
36. P. Benes, V. Vetvicka, M. Fusek, Cathepsin D—Many functions of one aspartic protease. *Crit. Rev. Oncol. Hematol.* **68**, 12–28 (2008).
37. A.-S. Bach, D. Derocq, V. Laurent-Matha, P. Montcourrier, S. Sebti, B. Orsetti, C. Theillet, C. Gongora, S. Pattingre, E. Ibing, P. Roger, L. K. Linares, T. Reinheckel, G. Meurice, F. J. Kaiser, C. Gespach, E. Liaudet-Coopman, Nuclear cathepsin D enhances TRPS1 transcriptional repressor function to regulate cell cycle progression and transformation in human breast cancer cells. *Oncotarget* **6**, 28084–28103 (2015).
38. N. Bidère, H. K. Lorenzo, S. Carmona, M. Laforge, F. Harper, C. Dumont, A. Senik, Cathepsin D triggers Bax activation, resulting in selective apoptosis-inducing factor (AIF) relocation in T lymphocytes entering the early commitment phase to apoptosis. *J. Biol. Chem.* **278**, 31401–31411 (2003).
39. M. Beaujouin, S. Baghdiguian, M. Glondu-Lassis, G. Berchem, E. Liaudet-Coopman, Overexpression of both catalytically active and -inactive cathepsin D by cancer cells enhances apoptosis-dependent chemo-sensitivity. *Oncogene* **25**, 1967–1973 (2006).
40. S. D. Hansen, J. B. Zuchero, R. D. Mullins, Cytoplasmic actin: Purification and single molecule assembly assays. *Methods Mol. Biol.* **1046**, 145–170 (2013).
41. S. Diment, M. S. Leech, P. D. Stahl, Cathepsin D is membrane-associated in macrophage endosomes. *J. Biol. Chem.* **263**, 6901–6907 (1988).
42. M. Heinrich, M. Wickel, W. Schneider-Brachert, C. Sandberg, J. Gahr, R. Schwandner, T. Weber, P. Saftig, C. Peters, J. Brunner, M. Krönke, S. Schütze, Cathepsin D targeted by acid sphingomyelinase-derived ceramide. *EMBO J.* **18**, 5252–5263 (1999).
43. P. Kirchner, M. Bourdenx, J. Madrigal-Matute, S. Tiano, A. Diaz, B. A. Bartholdy, B. Will, A. M. Cuervo, Proteome-wide analysis of chaperone-mediated autophagy targeting motifs. *PLOS Biol.* **17**, e3000301 (2019).

44. S. Kaushik, A. M. Cuervo, The coming of age of chaperone-mediated autophagy. *Nat. Rev. Mol. Cell Biol.* **19**, 365–381 (2018).

45. S. Ono, K. Mohri, K. Ono, Microscopic evidence that actin-interacting protein 1 actively disassembles actin-depolymerizing factor/cofilin-bound actin filaments. *J. Biol. Chem.* **279**, 14207–14212 (2004).

Citation: Y.-J. Liu, T. Zhang, D. Cheng, J. Yang, S. Chen, X. Wang, X. Li, D. Duan, H. Lou, L. Zhu, J. Luo, M. S. Ho, X.-D. Wang, S. Duan, Late endosomes promote microglia migration via cytosolic translocation of immature protease cathD. *Sci. Adv.* **6**, eaba5783 (2020).